ADVANCES IN ATMOSPHERIC SCIENCES, VOL. 30, NO. 3, 2013, 739–753

FGOALS-s2 Simulation of Upper-level Jet Streams over East Asia: Mean State Bias and Synoptic-scale Transient Eddy Activity

SONG Fengfei[1,2] (宋丰飞) and ZHOU Tianjun[*1,3] (周天军)

[1] *State Key Laboratory of Numerical Modeling for Atmospheric Sciences and Geophysical Fluid Dynamics, Institute of Atmospheric Physics, Chinese Academy of Sciences, Beijing* 100029

[2] *Graduate University of the Chinese Academy of Sciences, Beijing* 100049

[3] *Climate Change Research Center, Chinese Academy of Sciences, Beijing* 100029

(Received 25 June 2012; revised 8 November 2012)

ABSTRACT

Upper-level jet streams over East Asia simulated by the LASG/IAP coupled climate system model FGOALS-s2 were assessed, and the mean state bias explained in terms of synoptic-scale transient eddy activity (STEA). The results showed that the spatial distribution of the seasonal mean jet stream was reproduced well by the model, except that following a weaker meridional temperature gradient (MTG), the intensity of the jet stream was weaker than in National Centers for Environment Prediction (NCEP)/Department of Energy Atmospheric Model Inter-comparison Project II reanalysis data (NCEP2). Based on daily mean data, the jet core number was counted to identify the geographical border between the East Asian Subtropical Jet (EASJ) and the East Asian Polar-front Jet (EAPJ). The border is located over the Tibetan Plateau according to NCEP2 data, but was not evident in FGOALS-s2 simulations. The seasonal cycles of the jet streams were found to be reasonably reproduced, except that they shifted northward relative to reanalysis data in boreal summer owing to the northward shift of negative MTGs. To identify the reasons for mean state bias, the dynamical and thermal forcings of STEA on mean flow were examined with a focus on boreal winter. The dynamical and thermal forcings were estimated by extended Eliassen-Palm flux ($\boldsymbol{E}$) and transient heat flux, respectively. The results showed that the failure to reproduce the tripolar-pattern of the divergence of $\boldsymbol{E}$ over the jet regions led to an unsuccessful separation of the EASJ and EAPJ, while dynamical forcing contributed less to the weaker EASJ. In contrast, the weaker transient heat flux partly explained the weaker EASJ over the ocean.

Key words: FGOALS-s2, jet stream, synoptic-scale transient eddy activity, meridional temperature gradient, extended Eliaseen-Palm flux, transient heat flux

Citation: Song, F. F., and T. J. Zhou, 2013: FGOALS-s2 simulation of upper-level jet streams over East Asia: Mean state bias and synoptic-scale transient eddy activity. *Adv. Atmos. Sci.*, **30**(3), 739–753, doi: 10.1007/s00376-012-2212-7.

1. Introduction

The upper tropospheric jet streams, as important components of atmospheric circulation over East Asia, have great influence on regional climatic change (Liang and Wang, 1998; Jhun and Lee, 2004; Liao et al., 2004; Zhou et al., 2005; Du et al., 2008, 2009). The jet streams also play important roles in connecting climate change over the Atlantic–Europe region with that over East Asia. For example, the wintertime North Atlantic Oscillation (NAO) (for details of other abbreviations used in this paper, please see Table 1) affects cold season (boreal winter and spring) climate over East Asia through wave-train propagation along the jet streams (Watanabe, 2004; Yu and Zhou, 2004; Li et al., 2005; Xin et al., 2006; Yu and Zhou, 2007).

The jet streams over East Asia have two branches: the East Asian Subtropical Jet (EASJ) and the East Asian Polar-front Jet (EAPJ) (Sheng, 1986; Zou et al., 1990). In boreal winter, these two jet streams are lo-

*Corresponding author: ZHOU Tianjun, zhoutj@lasg.iap.ac.cn

Table 1. Abbreviations defined and used in the text.

Full names	Abbreviations
Synoptic-scale Transient Eddy Activity	STEA
Meridional Temperature Gradient	MTG
East Asian Subtropical Jet	EASJ
East Asian Polar-front Jet	EAPJ
Eliassen-Palm flux	$\boldsymbol{E}$
North Atlantic Oscillation	NAO
Tibetan Plateau	TP
Coupled Model Inter-comparison Program phase 5	CMIP5
Spectral Atmosphere Model of IAP LASG version 2	SAMIL2
LASG/IAP Climate Ocean Model version 2	LICOM2
Community Land Model version 3	CLM3
Community Sea Ice Model version 5	CISM5
National Center for Atmospheric Research	NCAR
National Centers for Environment Prediction	NCEP
Jet Core Number	JCN
Kinetic Energy	KE
Atmospheric Model Inter-comparison Program	AMIP
East Asian Winter Monsoon	EAWM

cated south and north of the Tibetan Plateau (TP), respectively. In boreal summer, the two jet streams can also be identified from daily data, but with different intensities and locations. The EAPJ in summer is weaker and located farther north than in winter (Zhang et al., 2008a). Since the EASJ is strong and stable, its seasonal evolution has received more attention in the past. Many previous studies have shown that the EASJ is stronger and shifts southward in winter compared to summer. There are transitions of the EASJ from south to north and vice versa in spring and autumn respectively, accompanied by transitions of the East Asian atmospheric circulation pattern (Tao et al., 1958; Yeh et al., 1958; Li et al., 2004; Zhang et al., 2006).

The seasonal evolution of the EASJ can be well depicted by monthly mean data, but it is not suitable to study the EAPJ in this way owing to its transient characteristics (Lee and Kim, 2003). Meanwhile, since the intensity of monthly mean wind gradually decreases from the stronger EASJ to the weaker EAPJ, it is difficult to identify the border dividing the two. Therefore, high-frequency datasets have been used to identify the border between the EASJ and EAPJ and the seasonal evolution of the EAPJ (Koch et al., 2006; Strong and Davis, 2007, 2008; Schiemann et al., 2009; Ren et al., 2010a).

Although the jet streams are considered part of large-scale circulation, they are closely connected to synoptic-scale transient eddy activity (STEA). In boreal winter, there are two branches of STEA over East Asia. The weaker (or stronger) STEA branch corresponds to a stronger (or weaker) EASJ (or EAPJ) (Ren et al., 2010b). However, a stronger (or weaker) jet stream is also accompanied by stronger (or weaker) STEA from the perspective of seasonal cycles of the climatological jet stream (Wu et al., 2006). The association between STEA and jet stream variations is attributed to either dynamical (Carillo et al., 2000; Ren and Zhang, 2007) or thermal feedback (Xiang and Yang, 2012).

Given the importance of these jet streams in East Asian climate, how to improve their simulation has been a focus of the climate modeling community. While their structures, locations and seasonal evolutions are reproduced well by many climate models, their intensities are not, partly due to bias in the simulation of meridional temperature gradients (MTGs) (Zhang and Kuang, 2006; Guo et al., 2008; Zhang et al., 2008b; Cai et al., 2011). Biases in oceanic forcing and poor representation of TP topography may also contribute (Manabe and Terpstra, 1974; Liu and Tang, 1996; Kuang et al., 2009). However, the influences of STEA dynamical and thermal feedback mechanisms on the bias of mean state jet streams are not well understood. Accordingly, the present reported study aimed to evaluate the performance of the Flexible Global Ocean-Atmosphere-Land System model, Spectral Version 2 (FGOALS-s2), a coupled climate system model developed by the State Key Laboratory of Numerical Modeling for Atmospheric Sciences and Geophysical Fluid Dynamics/Institute of Atmospheric Physics (LASG/IAP) over the last five years (Bao et al., 2013), in simulating upper-level jet streams and associated STEA over East Asia. The FGOALS-s2 model has been participating in the Coupled Model Inter-comparison Program phase 5 (CMIP5) for IPCC Fifth Assessment Report (AR5), but the performance

of the model in simulating jet streams and STEA processes have yet to be assessed. The present results are thus a useful reference for the future development and improvement of the FGOALS model program.

The remainder of the paper is organized as follows. Section 2 introduces the model, reanalysis dataset, and analysis methods. Model results are compared to reanalysis data in section 3. And finally, section 4 summarizes the major conclusions.

2. Model, reanalysis dataset and methods

2.1 *Model*

FGOALS-s2 is a state-of-the-art global coupled climate model developed by the LASG/IAP and has been involved in the CMIP5 experiment for IPCC AR5 (Bao et al., 2013). The FGOALS-s2 is a new version of FGOALS-s1, a coupled climate system model that has been widely used in climate variability studies (Zhou et al., 2005; Bao et al., 2010; Zhang et al., 2010; Yang et al., 2012). The atmospheric component of FGOALS-s2 is the Spectral Atmosphere Model of IAP LASG, Version 2 (SAMIL2), which employs a hybrid-coordinate system with 26 vertical layers (L26), and is rhomboidally truncated at wave-number 42 in the horizontal direction (R42), roughly on a 2.8° (lat)×1.66° (lon) Gaussian grid. The oceanic component is the LASG IAP Climate system Ocean Model, version 2 (LICOM2), with a horizontal resolution of about 1°×1° over the extra-tropical region and 0.5°×0.5° over the tropics, and 30 vertical levels. The land and ice components are the Community Land Model version 3 (CLM3) and Community Sea Ice Model version 5 (CSIM5), respectively. The four components are coupled by a flux coupler module from the National Center for Atmospheric Research (NCAR). For details of FGOALS-s2 and its general performance, readers are referred to Bao et al. (2013).

In this study, the monthly and daily outputs of FGOALS-s2 historical simulations were analyzed. The selected variables included zonal wind, meridional wind and air temperature. For an analysis of the model's performance in reproducing 20th century global and regional surface air temperature evolution, readers are referred to Zhou et al. (2013).

2.2 *Reanalysis dataset*

In order to evaluate the model's performance, monthly and daily variables from the National Centers for Environment Prediction (NCEP)/Department of Energy Atmospheric Model Inter-comparison Project II reanalysis data (NCEP2) (Kanamitsu et al., 2002) were used. The data are available on a 2.5°×2.5° grid and our analysis focused on the period 1979–2005. We refer to winter as December–February (DJF) and summer as June–August (JJA).

2.3 *Analysis method*

To identify the border between the EASJ and EAPJ, the number of jet cores at each grid point (i.e. the jet core number; JCN) was calculated using daily 250-hPa zonal wind fields. This vertical level was selected because of the lack of 200-hPa daily outputs from the model. The definition of the jet core in this study was as follows: (1) zonal wind speed was $\geqslant$20 m s^{-1}; and (2) zonal wind speed was the local maximum of the surrounding eight grid points. In comparison to previous definitions (Zhang et al., 2008b; Ren et al., 2010a, b), the zonal wind speed rather than total wind speed was used here to highlight the zonal wind. As will be shown later, since the jet stream in the model is weaker than that in the reanalysis, the zonal wind speed limit was chosen as 20 m s^{-1} in our analysis except for special remarks.

To represent the thermal configuration of the jet streams, the MTG was calculated using air temperature in the south grid minus that in the north grid by the central difference method. The jet axis, defined as the latitude of maximum zonal wind in the meridional direction from 10°N to 60°N along selected longitudes, was used to show the seasonal evolution of the jet streams clearly.

STEA was measured by eddy kinetic energy (KE):

$$K_e = (\overline{u'^2 + v'^2})/2 \,, \tag{1}$$

where u' and v' denote zonal and meridional wind through 2.5–8-day band-pass filtering (Ren et al., 2010b), respectively. The overbar indicates the time-mean over a specified period. The u', v' and overbar have the same meanings in the following formulas.

The extended Eliassen-Palm flux ($\boldsymbol{E}$), developed by Hoskins et al. (1983), can effectively highlight the dynamical interaction between transient eddies and the mean flow. According to Hoskins et al. (1983), the horizontal $\boldsymbol{E}$ vector is defined as

$$\boldsymbol{E} = (\overline{v'^2 - u'^2}, -\overline{u'v'}) \,. \tag{2}$$

The divergence (or convergence) of the $\boldsymbol{E}$ vector corresponds to an increase (or decrease) of the westerly mean flow through a dynamical forcing on the mean horizontal circulation (Carillo et al., 2000). The thermal forcing on the mean horizontal circulation is represented by the transient heat flux ($\overline{u'T'}, \overline{v'T'}$), where T' denotes air temperature through 2.5–8-day band-pass filtering. According to the thermodynamical equation, the convergence of the transient heat flux is proportional to the mean air temperature change.

3. Results

In the following analysis, we firstly examine the performance of FGOALS-s2 in simulating the climatology of jet streams over East Asia, both in winter and summer. The JCN results, calculated to divide the EASJ and EAPJ in winter based on daily mean datasets, are reported. Meanwhile, the model's performance in reproducing the seasonal evolution of the jet streams is evaluated. The reasons for model bias in the simulation of the jet streams are investigated from the perspective of STEA. Since the EASJ weakens and the EAPJ almost disappears in summer, we mainly focus on winter in the analysis.

3.1 *Climatology of the jet streams*

The climatological distribution of jet streams over East Asia at 200 hPa derived from NCEP2 data and FGOALS-s2 simulations are shown in Fig. 1. Before calculating the difference between the two, zonal wind in the model was interpolated to the 2.5°×2.5° grid. In winter, a maximum zonal wind band along 30°N is evident in the NCEP2 data, commonly called the EASJ. The center is located over the ocean east of Japan, with wind speed >70 m s^{-1}. The northward ridge of zonal wind over the land at 50°N is evident, indicative of another zonal wind center around this latitude. This inconspicuous center is often called the EAPJ. As shown in Fig. 1a, the geographical border dividing the EASJ from EAPJ is not obvious in monthly mean fields. In summer, the EASJ shifts northward to 40°N. The EAPJ cannot be seen from the seasonal mean data, but can still be identified from the daily mean data (Zhang et al., 2008b). The main center also moves from the ocean to the land, with only about half the intensity of the winter center (Fig. 1b).

The winter zonal wind in the FGOALS-s2 results showed a spatial pattern similar to that in the NCEP2 data, but with some obvious biases. The largest deficiency was the significant underestimation of zonal wind along the EASJ, especially over the ocean (Fig. 1e). The positive bias center, consistent with the jet center, was about 15 m s^{-1} weaker than in NCEP2. Another bias was the overestimation of

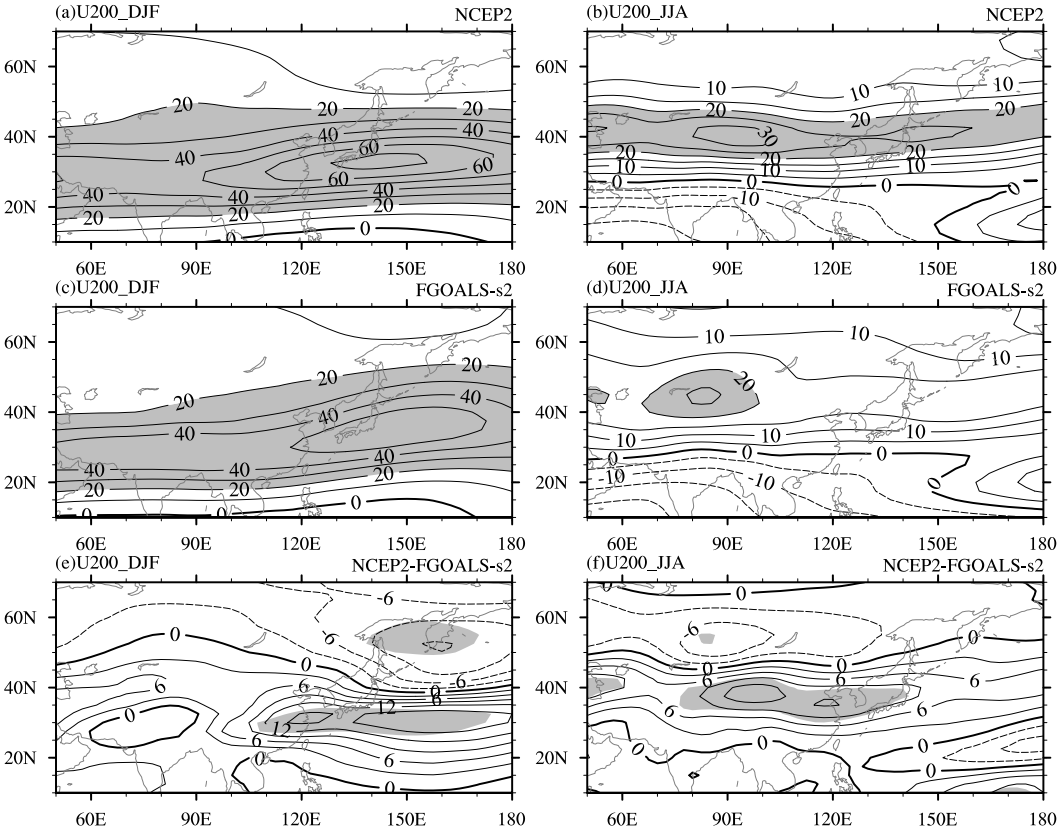

Fig. 1. Climatological zonal wind (units: m s^{-1}) at 200 hPa in winter (DJF mean, left panels) and summer (JJA mean, right panels) based on NCEP2 (top panels), FGOALS-s2 (middle panels) and their differences (bottom panels). Shaded regions are where wind speed is >20 m s^{-1}. Shaded regions in the bottom panel are where the differences are statistically significant at the 10% level.

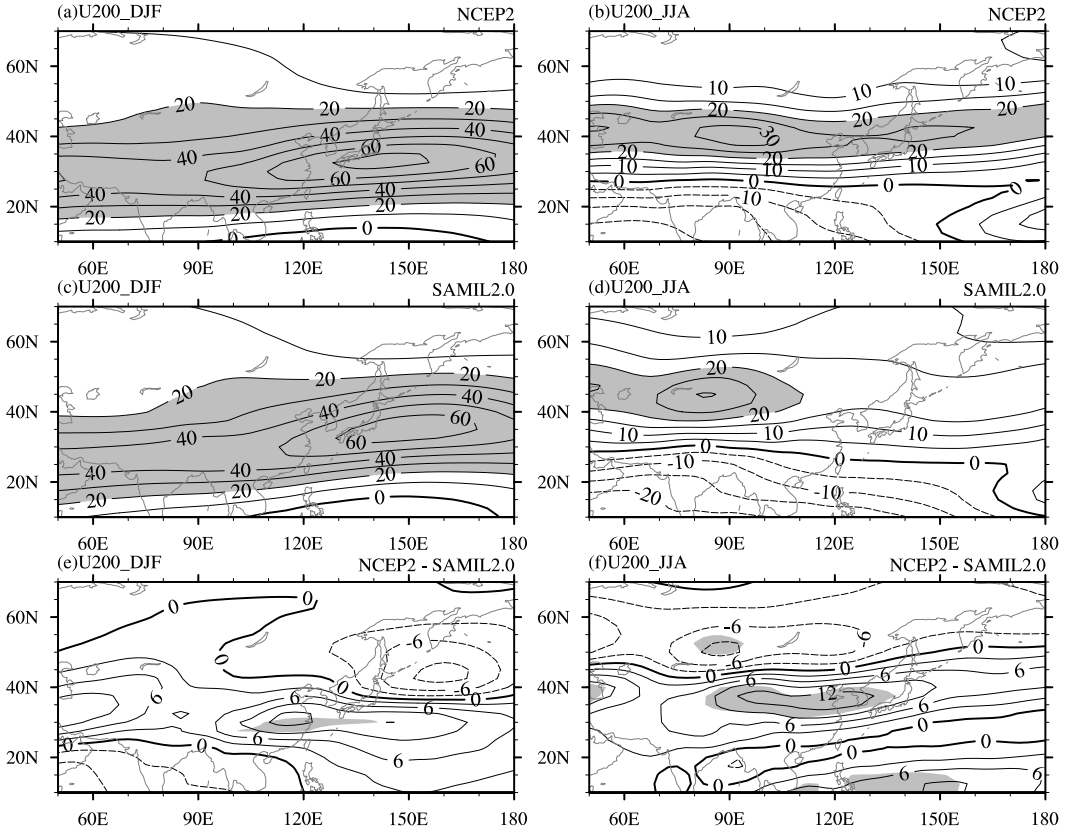

Fig. 2. The same as Fig. 1, but for SAMIL2.0 instead of FGOALS-s2.

zonal wind north of 45°N, which was about 12 m s^{-1} stronger south of Kamchatka Peninsula. In summer, the jet stream was much weaker than in NCEP2 and shifted more westward. Similar to winter, there were also two main biases. One was along the jet stream, which was about 12 m s^{-1} weaker than in NCEP2 in the center. The other was located to the north of the jet, which was about 6 m s^{-1} stronger than in the reanalysis. Both in winter and summer, the biases of zonal wind exhibited a dipole pattern. The positive center of the dipole pattern coincided well with the jet stream, while the negative lobe was located in the north of the jet.

Guo et al. (2008) evaluated the performance of the atmospheric component of FGOALS-s2 (SAMIL) in simulating the climatological mean state of the upper-level jet streams over East Asia. In order to understand to what extent air–sea coupling affects the simulation of the upper-level jet streams, we compared the jet streams simulated by FGOALS-s2 AMIP (Atmospheric Model Inter-comparison Program) and historical simulations (Fig. 2). The locations of the jet streams in the AMIP simulation were similar to those in the historical simulation. However, compared to the historical simulation, the intensity of the jet streams in the AMIP simulation was much stronger in winter but somewhat weaker in summer. Hence, in comparison with the historical simulation, the intensity of the jet streams in the AMIP simulation was more comparable to NCEP2 in winter, but less comparable in summer, which was consistent with the results reported by Guo et al. (2008). This indicates that the effect of air–sea coupling is seasonally dependent and may be related to the seasonal locations of jet streams.

As shown in Fig. 1, the geographical border dividing the EASJ from the EAPJ is not obvious in the monthly mean data. Hence, the climatological distribution of the JCN at 250 hPa was plotted in Fig. 3. The JCN zonal band is located along 30°N and shifts northward over the ocean. The most obvious JCN centers are coincident with the zonal wind maximum from the monthly mean data. Besides these centers, there are JCN centers along the EASJ south of the TP. The JCN maximum band north of the TP is also obvious, corresponding to the EAPJ. The minimum JCNs are evident between these two lobes, extending zonally from the western to the eastern side of the TP. This region is considered as the border between the

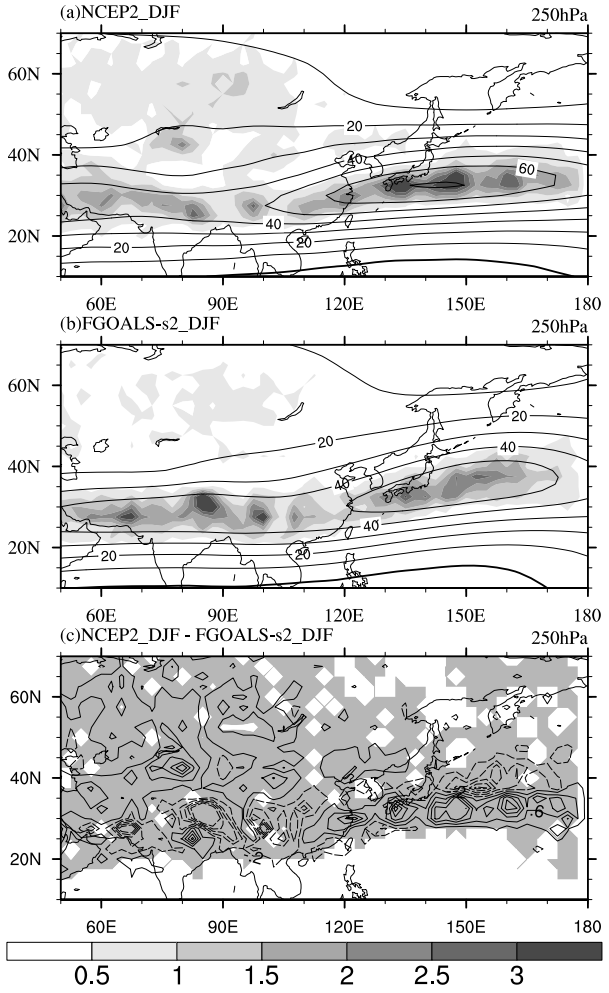

Fig. 3. Climatological distributions of the JCN (shaded) and zonal wind (contour, units: m s^{-1}) at 250 hPa based on (a) NCEP2 and (b) FGOALS-s2 in winter. The differences between (a) and (b) are shown in (c). Shaded regions in (c) are where the differences are statistically significant at the 10% level.

EASJ and EAPJ in winter. Hence, the EAPJ can be distinguished from the EASJ from the daily mean data, with the border region over the TP. In FGOALS-s2, the JCN centers over the ocean were not as strong as those in NCEP2, which was consistent with the weaker magnitude of zonal wind. However, the centers south of the TP were stronger than those over the ocean–even stronger than their counterparts in NCEP2. In the EAPJ region, the maximum JCN band was not reproduced well, which is also reflected in the difference field in Fig. 3c. The failure to reproduce the border between the EASJ and EAPJ is related to the underestimation of jet streams in FGOALS-s2.

To show the vertical structure of jet streams, three typical longitudes (90°E, 120°E and 140°E) were chosen as representatives of the land, the transition region and the ocean, respectively. The height–latitude sections of zonal wind and the MTGs are shown in Figs. 4 and 5 for winter and summer, respectively. In winter (Fig. 4), the strongest zonal wind occurs around 30°N at 200 hPa, accompanied by strong positive (or negative) MTGs below (or above) the jet center. This zonal wind-MTG configuration is consistent with the thermal wind principle (Zhang et al., 2006), in which the vertical shear of the zonal wind is proportional to the MTG. The westerly wind is gradually enhanced from west to east and reaches the maximum at 140°E. The MTG shows a similar zonal change. Similar features were also evident in FGOALS-s2, but the intensity was much weaker than in NCEP2. In summer (Fig. 5), the maximum zonal wind also appeared at 200 hPa but moved to about 40°N. From west to east, the westerly wind and MTGs gradually decreased – a situation which was opposite to that in winter. Although zonal wind-MTG structure was reproduced in FGOALS-s2, the weaker jet stream shifted more northward and covered a wider meridional range.

To reveal the zonal variations of jet streams, zonal wind and MTGs along 32°N and 42°N, corresponding to the locations of the EASJ in winter and summer, respectively, are shown in Fig. 6. Although there are zonal wind centers over land and ocean both in winter and summer, the main centers of the EASJ are located over the ocean and land for winter and summer, respectively. The main center in winter is located along 140°E at 200 hPa, with the zonal wind speed >70 m s^{-1}. During summer, however, the main center becomes weaker and splits into two parts. In FGOALS-s2, zonal wind and MTGs were weaker and more uniform. Except for a more eastward shift of the western center in winter, the zonal wind centers in winter and summer were reproduced well.

3.2 *Seasonal evolution of jet streams*

Both the intensity and locations of jet streams show robust seasonal cycles. The seasonal evolutions of zonal wind, the jet axis and MTGs at 200 hPa are shown in Fig. 7. The jet along 90°E settles around 28°N from January to April and jumps sharply to 38°N in May. It stays around 40°N for about five months (from May to September) and again moves southward to about 30°N rapidly. The jet along the other two longitudes shows a similar seasonal evolution, but in a more gradual way. A similar meridional shift is seen in MTG as the jet. In FGOALS-s2, the sharp northward shift of the jet along 90°E in May was captured well, but the sharp southward shift in October was not reproduced (Fig. 7d). Along all three longitudes, the

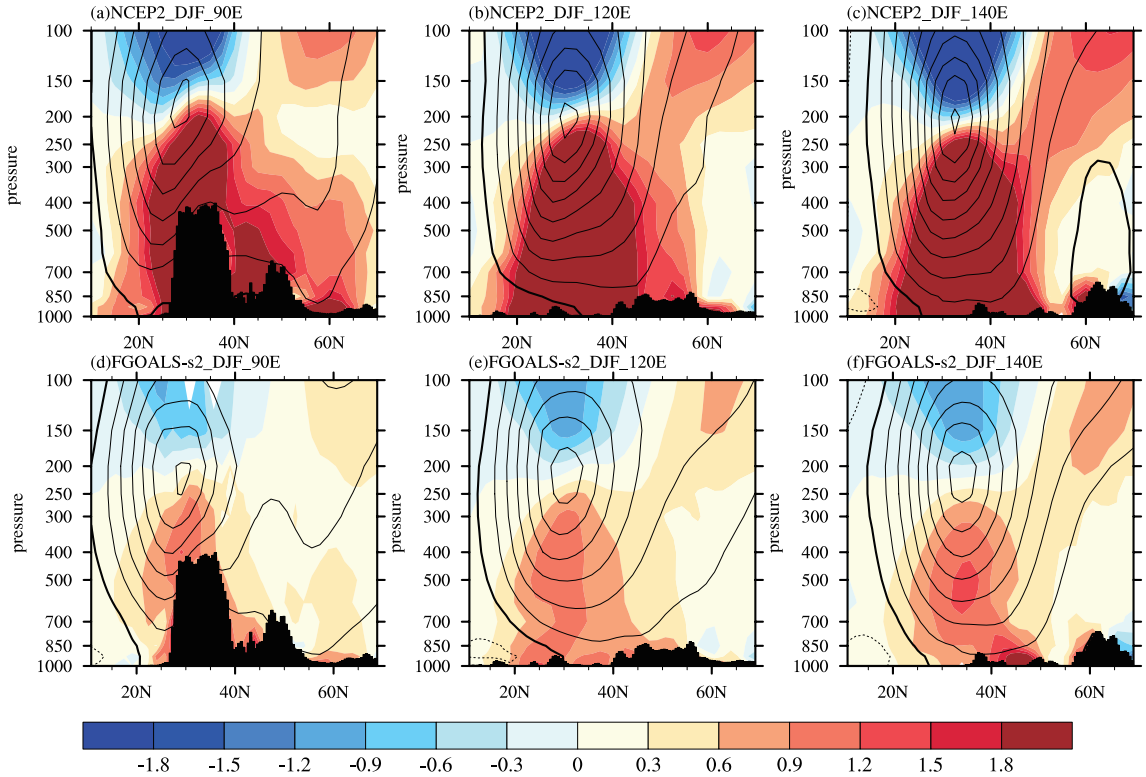

Fig. 4. Latitude–height cross sections of zonal wind (contour, units: m s^{-1}) and meridional temperature gradient (shaded, units: K) in winter along 90°E (left panels), 120°E (middle panels) and 140°E (right panels) based on NCEP2 (top panels) and FGOALS-s2 (bottom panels). The solid (or dashed) line represents positive (or negative) values, respectively. The bold line indicates the zero values and the contour interval is 8 m s^{-1}.

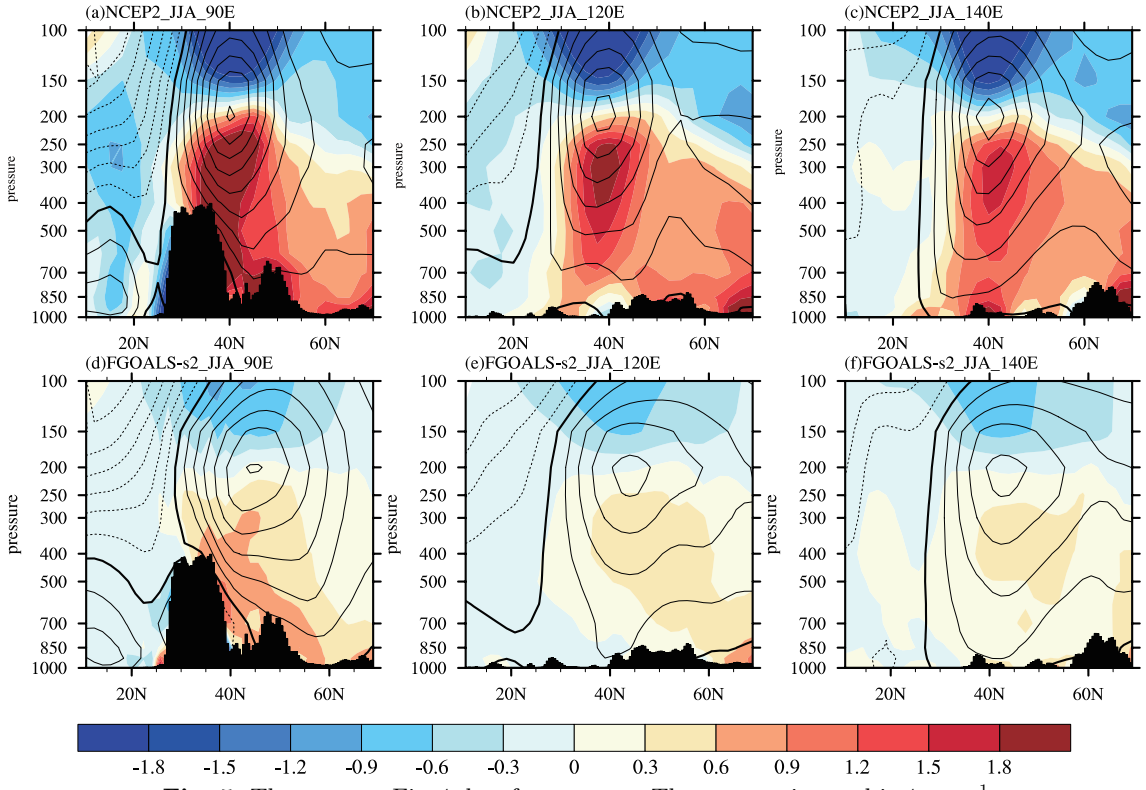

Fig. 5. The same as Fig. 4, but for summer. The contour interval is 4 m s^{-1}.

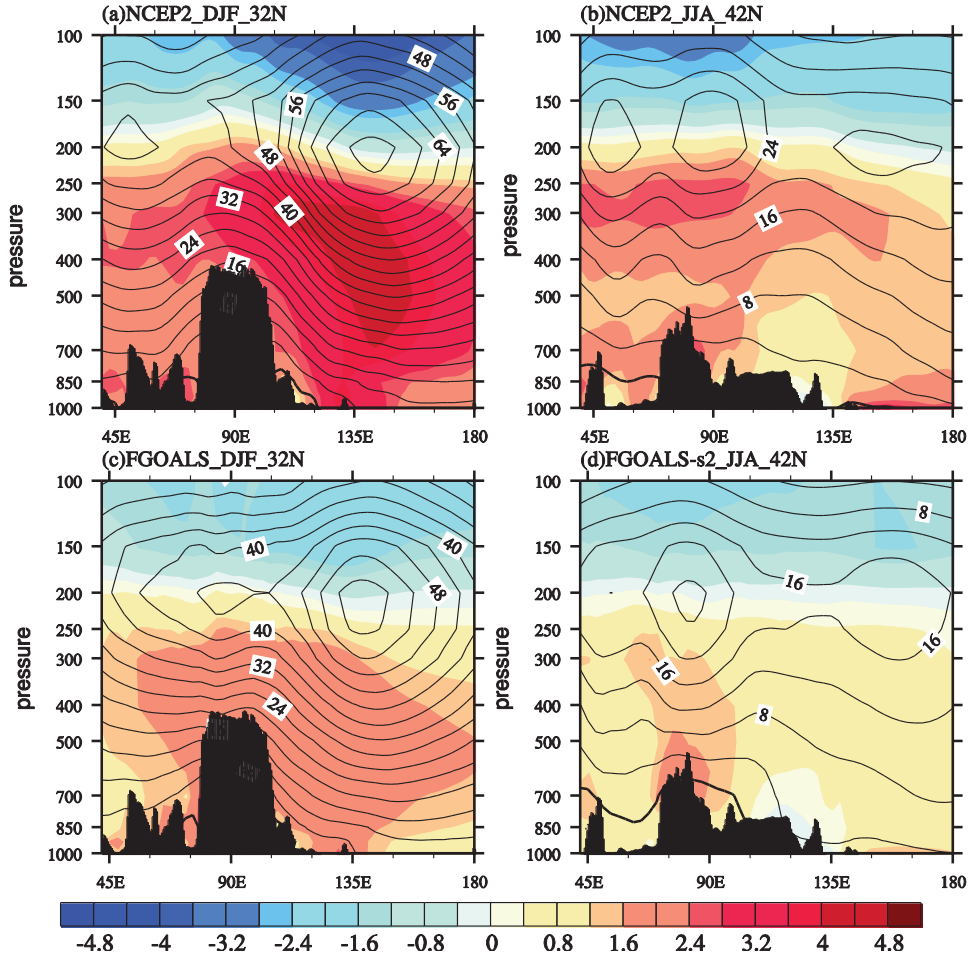

Fig. 6. Longitude–height cross sections of zonal wind (contour, units: m s^{-1}) and meridional temperature gradient (shaded, units: K) along 32°N and 42°N in winter (left panels) and summer (right panels), respectively, based on NCEP2 (top panels) and FGOALS-s2 (bottom panels).

jet moved more northward in summer, as a result of a greater northward shift of the negative MTGs.

To show the seasonal evolution of the jet stream more clearly, the jet core's position and magnitude at 200 hPa in different months are shown in Fig. 8. When calculating the jet core's position, the zonal wind limit was set to 30 m s^{-1} for NCEP2, but kept at 20 m s^{-1} in the model. The jet core is located east of 130°E for most months and shifts westward to about 90°E in July and August only (Fig. 8a). In contrast, the meridional shift of the jet core is more evident. The jet core stays stationary around 32.5°N during January–April but jumps northward to 40°N in May. From May to October, the jet core is located north of 37°N, and reaches 45°N as the northernmost latitude in September. The southward shift of the jet core occurs during September–November and stays unchanged from November to December. The wind speed of the jet core in winter is greater than in summer, with the greatest (or smallest) speed in January (or July). Except for June, the simulated jet core longitude in each month was analogous to NCEP2. The latitude of the jet core in FGOALS-s2 was located farther northward than in NCEP2 for most months. The magnitude of the jet core was smaller than in NCEP2 in each month, but the seasonal evolutions in the model and NCEP2 were in phase.

The interannual variability of the three quantities shown in Fig. 8 in boreal winter was also investigated. Considering the winter season, the zonal wind limit to determine the jet core was set to 50 m s^{-1}. The standard deviations of the longitudes, latitudes and zonal wind speed of the jet core were 4.83 (or 6.63), 1.21 (or 2.17) and 4.13 (or 3.92) respectively in NCEP2 (or FGOALS-s2). Correspondingly, the three quantities for model-observation differences were 5.27, 1.07 and

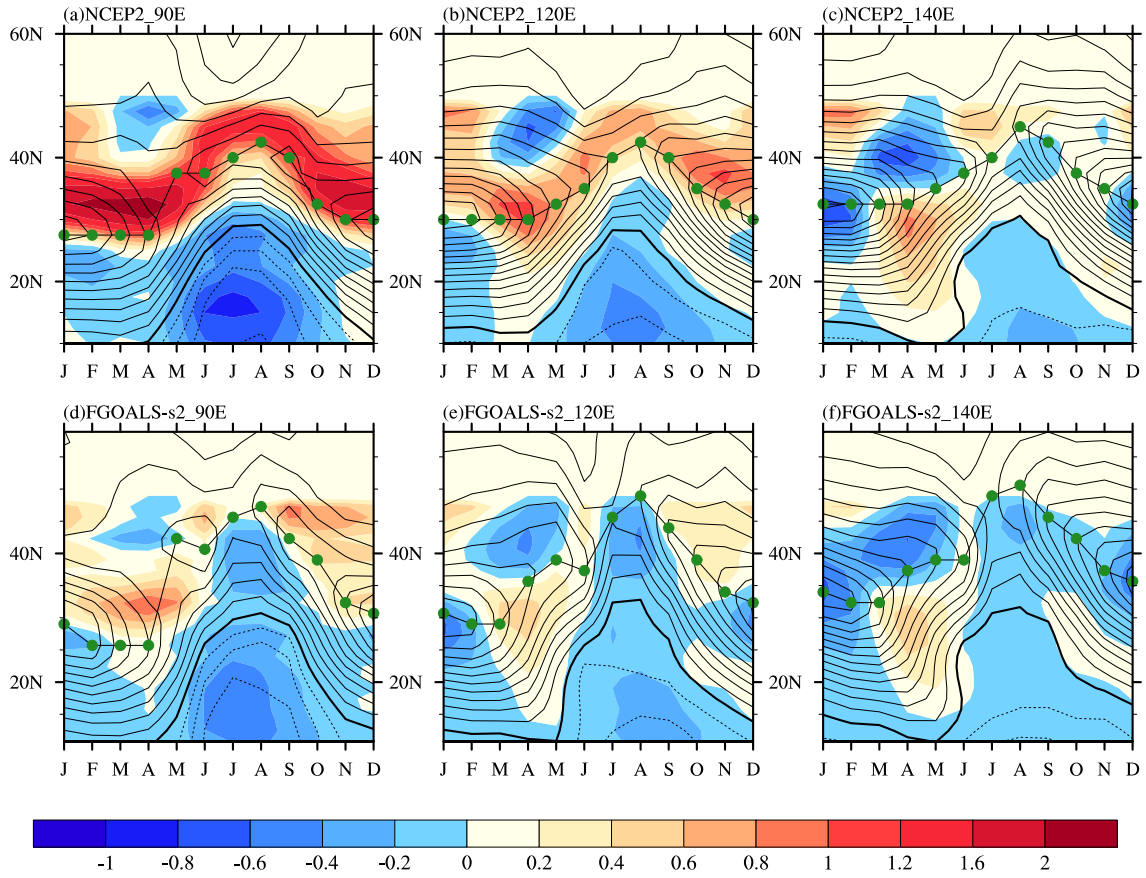

Fig. 7. Latitude–month cross sections of zonal wind (contour, units: m s^{-1}) and meridional temperature gradient (shaded, units: K) at 200 hPa along 90°E (left panels), 120°E (middle panels) and 140°E (right panels) The thick solid lines indicate the jet axis. The solid (or dashed) line represents positive (or negative) values, respectively. The bold line indicates the zero values and the contour interval is 4 m s^{-1}.

4.35. Hence, the interannual variability of the three quantities was comparable to the model-observation difference. This indicates the model bias may be concealed and not separated easily from the interannual variability.

3.3 *STEA*

The above analysis showed that the jet streams in FGOALS-s2 were weaker than in NCEP2, and the JCN center over the EAPJ region was not evident in the simulation. In the following analysis, we examine the connections between the bias in the mean state of zonal wind and STEA. To ensure that the feedback mechanisms are based on a reasonable STEA, we begin our analysis from the evaluation of STEA simulation. The climatological distributions of STEA in NCEP2 and FGOALS-s2 are compared in Fig. 9. The most obvious feature of the reanalysis is an enormous STEA center over the North Pacific Ocean, indicative of a storm track over the region. The STEA over East Asia shows an omega shape and there is a ridge over the EAPJ region. The primary features of STEA were captured well in the FGOALS-s2 simulation, except that the magnitude was generally smaller than in the reanalysis (Fig. 9c).

To show the vertical structure of STEA, the STEA along 90°E and 140°E is shown in Fig. 10. There are two centers along 90°E: one along 30°N and the other along 57°N. The northern center is stronger than its southern counterpart. This is consistent with previous studies, which claim that a stronger (or weaker) EASJ (or EAPJ) corresponds to a weaker (or stronger) STEA branch (Ren et al., 2010b). The two STEA centers merge together over the ocean along 42°N. Although the STEA along 90°E at 40°N and the STEA along 140°E at 50°N were much smaller than in NCEP2 (Figs. 10e and f), the vertical structure of STEA was reproduced well by FGOALS-s2. Generally, the horizontal distributions and vertical structures of STEA were reproduced well, which adds confidence to

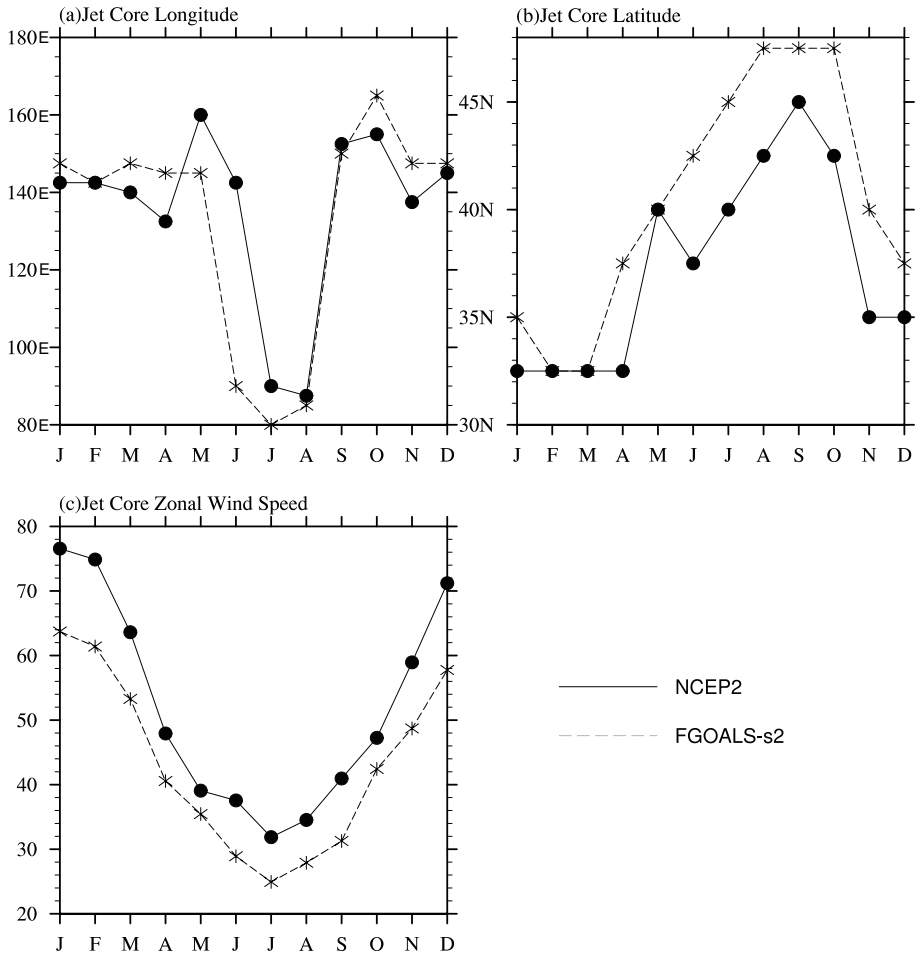

Fig. 8. Seasonal evolution of (a) longitude, (b) latitude and (c) zonal wind speed (units: m s^{-1}) of the westerly jet core based on NCEP2 (solid line) and FGOALS-s2 (dashed line).

the discussion on the feedback between the mean jet and STEA.

The STEA is connected to the mean flow by effectively transporting momentum and heat. To reveal the dynamical feedback of STEA on the jet, the horizontal distribution of $\boldsymbol{E}$ and its divergence are shown in Fig. 11. Over the two centers of STEA (see Fig. 10), $\boldsymbol{E}$ is also strong and divergent from 70°E to 110°E, contributing to an enhancement of the westerly wind and the formation of the EASJ and EAPJ. A strong convergence of $\boldsymbol{E}$ is seen between these two divergent regions, forming a tripolar pattern. This tripolar pattern favors the separation between the EASJ and EAPJ. An intense dipole pattern in the divergence field of $\boldsymbol{E}$ over the polar-front zone is evident, acting as a forcing to an increase (or decrease) of zonal wind north of (or along) the jet. The tripolar pattern over land was not simulated reasonably, which may contribute to the unsuccessful separation of the two jet streams (Fig. 11c). The dipole pattern was reproduced with a weaker negative center (Fig. 11c), indicating a weaker forcing on the mean flow to reduce the jet. Hence, the underestimated jet over the ocean may not be related to the dynamical feedback from STEA.

Besides the dynamical forcing on the jet, STEA can also affect the mean temperature field by heat flux transport, and indirectly induce a change of the jet. To examine this hypothesis, the climatological distributions of transient heat flux and its divergence are shown in Fig. 12. The most significant feature is a dipole pattern over the North Pacific Ocean, corresponding to the storm track. This pattern extends to eastern China with strong eastward heat flux. The simulated dipole pattern covers a narrower zonal range, with weaker magnitude and an eastward shift. The eastward heat flux and associated divergence field over eastern China are weaker. The difference between NCEP2 and FGOALS-s2 formed a similar pattern as

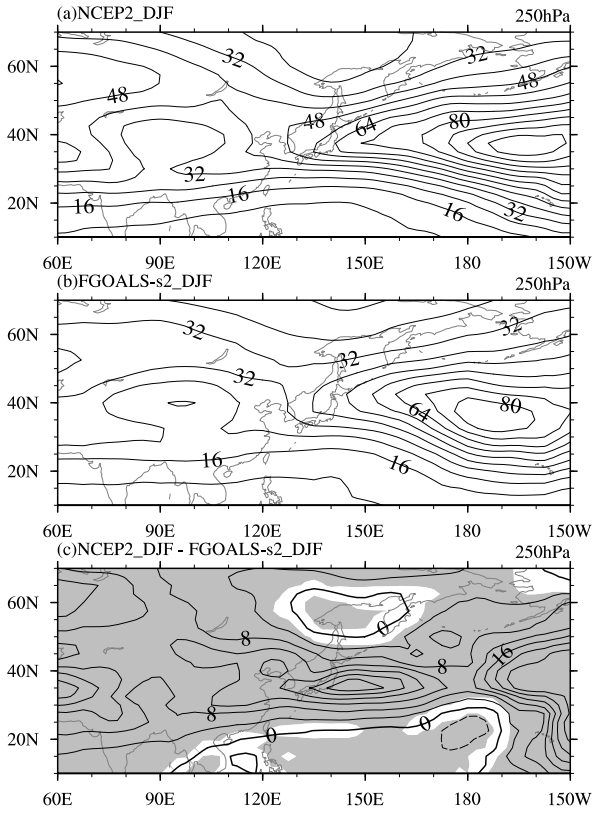

Fig. 9. Climatological distributions of STEA (units: $m^2\ s^{-2}$) at 250 hPa in winter based on (a) NCEP2 and (b) FGOALS-s2. The difference between (a) and (b) is shown in (c). Shaded regions in (c) are where the differences are statistically significant at the 10% level.

the climatological distribution over the storm track, indicating an underestimation of heat flux in the model (Fig. 12c). The divergence distribution of heat flux over land north of 40°N was reproduced well, albeit with a stronger northward heat flux. Hence, we deduce that transient heat flux transport may not be responsible for the EAPJ simulation bias, but contributes to the EASJ bias over the ocean.

4. Discussion and conclusion

The performance of FGOALS-s2 in simulating the upper-level jet streams and associated STEA over East Asia was evaluated. The historical simulation results were compared to NCEP2 reanalysis data. The horizontal distribution and vertical structure of the climatological jet stream were examined. The seasonal evolution of the jet axis, MTG and jet core was investigated. Based on daily mean datasets, simulated STEA and its dynamical and thermal forcing on the jet streams were assessed. The major conclusions from this work can be summarized as follows:

(1) The climatology of jet streams was reproduced well by FGOALS-s2 both in winter and summer, although with a weaker magnitude owing to the weaker MTG. Compared to the historical simulation, the intensity of the jet streams in the AMIP simulation was much stronger in winter but somewhat weaker in summer. Based on daily mean datasets, the JCN in winter was calculated to identify the geographical border between the EASJ and EAPJ. The separation border identified from NCEP2 data was located over the TP. However, the EASJ and EAPJ could not be separated well by FGOALS-s2. This failure may be attributable to the underestimation of zonal wind in the model.

(2) The seasonal cycles of the jet streams in the model were assessed by the jet axis and core. The simulated evolutions of the jet axis were analogous to NCEP2 data. The sharp northward shift of the jet along 90°E in May was simulated well, but the sharp southward shift in October was not reproduced. The other deficiency was that the simulated jet shifted farther northward in summer owing to a more northward shift of the negative MTGs. The longitudes of the jet core in each month were captured well, except in August, but the latitudes of the jet core were located farther northward as the jet axis. The speeds of the jet core in all months were smaller than in NCEP2 data, indicative of a systematic model bias.

(3) The model reproduced well the climatology of STEA. The feedback mechanisms between the mean jet and STEA were investigated. The dynamical forcing of STEA on the mean flow was represented by the extended Eliassen-Palm flux ($\boldsymbol{E}$) and its divergence. The divergence of $\boldsymbol{E}$ occurs over the EASJ and EAPJ region and there is an intense convergence between these two jet streams in the NCEP2 data, forming a tripolar pattern. This tripolar pattern favors the separation of these two jet streams. FGOALS-s2 failed to capture this tripolar pattern, indicating that the simulated bias of the dynamical forcing from STEA may be responsible for the unsuccessful separation of the two jet streams. The weaker simulated center of the convergence over the ocean indicates a weaker forcing on the mean flow to reduce the jet. Hence, the dynamical forcing of STEA may not contribute to the underestimated jet over the ocean. The thermal forcing of STEA was measured by the transient heat flux. In the model, the weaker and more eastward heat flux divergence field led to a colder air temperature, resulting in the weaker zonal wind. Hence, the bias in transient heat flux simulation well explains the weaker-than-reanalysis jet over the ocean.

This paper has discussed the mean state bias of the East Asian jet streams in FGOALS-s2 from the perspective of STEA. We have pointed out that the interactions between STEA and the jet streams (in-

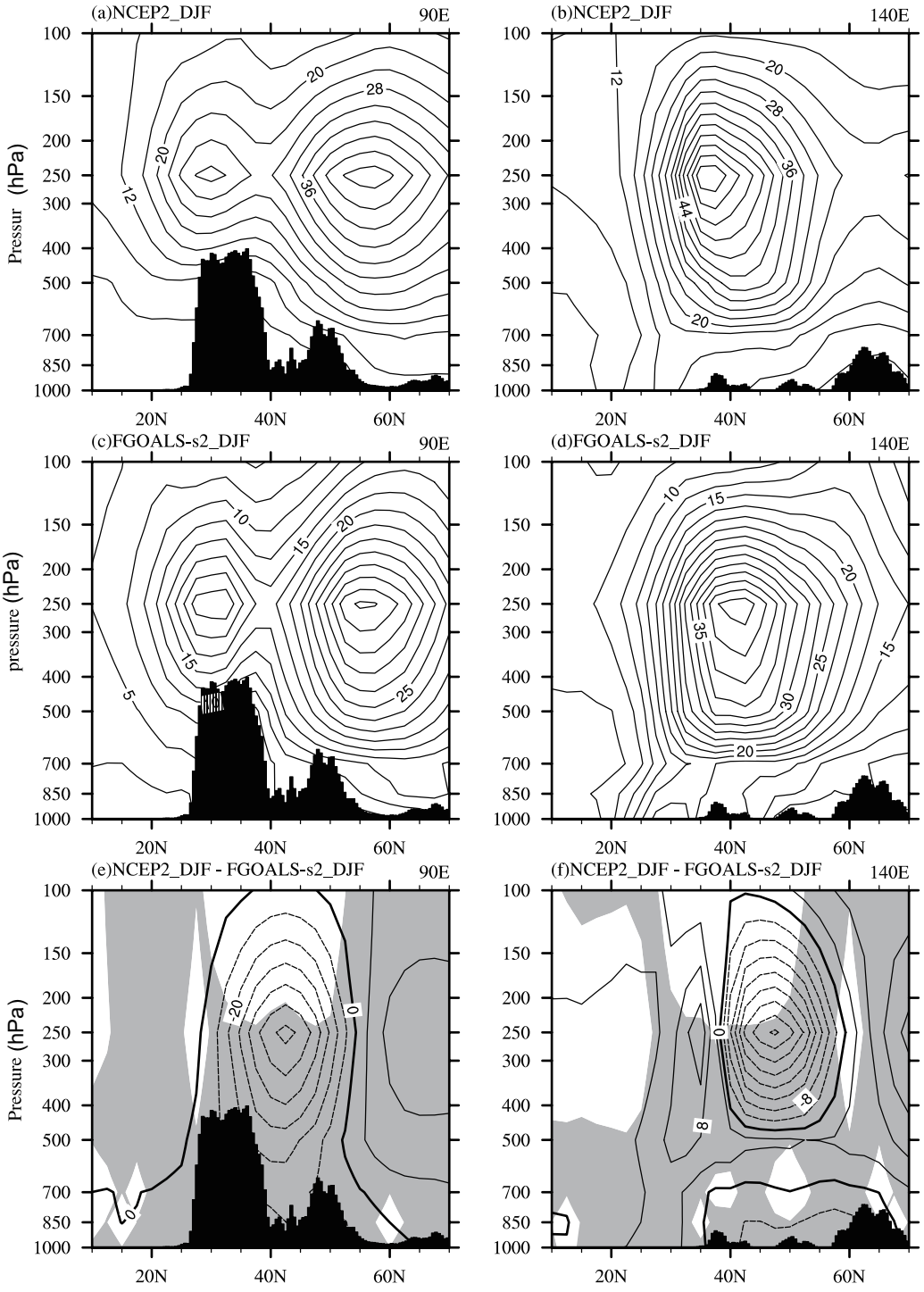

Fig. 10. Latitude–height cross sections of STEA (units: $m^2\ s^{-2}$) along 90°E (left panels) and 140°E (right panels) based on (a, b) NCEP2, (c, d) FGOALS-s2 and (e, f) the differences between NCEP2 and FGOALS-s2. Shaded regions in the bottom panel are where the differences are statistically significant at the 10% level.

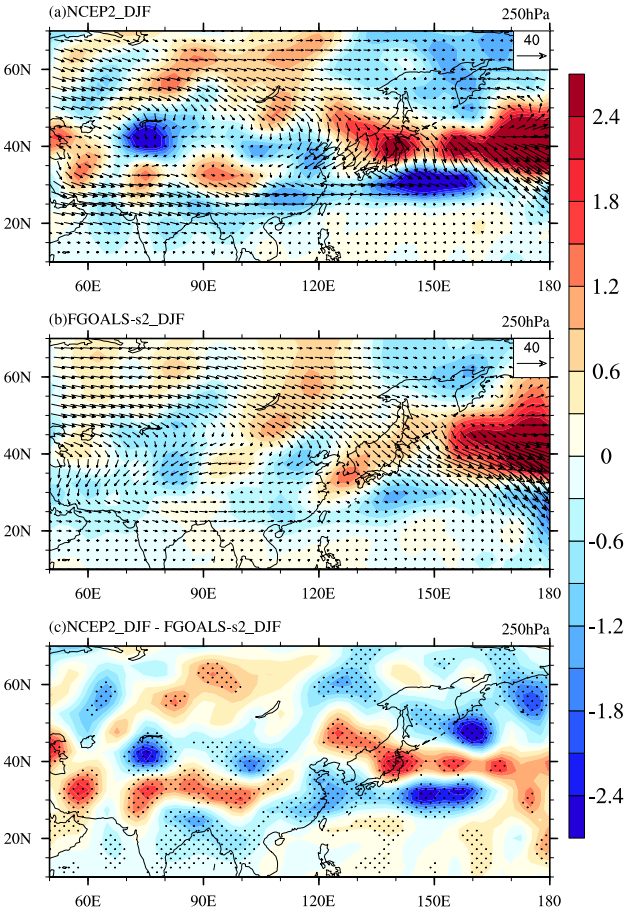

Fig. 11. The extended Eliasssen-Palm Flux (vectors, units: $m^2\ s^{-2}$) and its divergence (shaded, units: 10^{-5} $m\ s^{-2}$) at 250 hPa based on (a) NCEP2 and (b) FGOALS-s2. The difference of the divergence between NCEP2 and FGOALS-s2 is shown in (c). The dotted regions are where the differences are statistically significant at the 10% level.

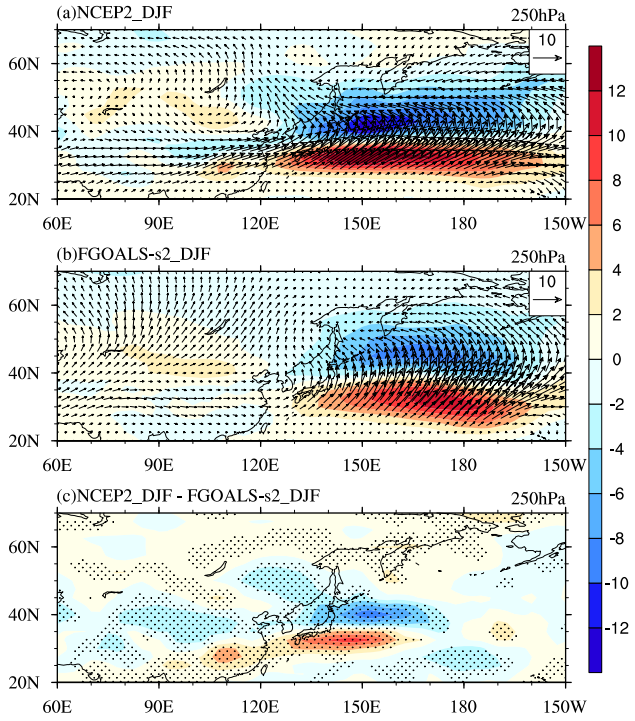

Fig. 12. Climatological distributions of synoptic-scale transient heat flux (vectors, units: $K\ m^{-1}$) and its divergence (shaded, units: 10^{-5} $K\ s^{-1}$) at 250 hPa based on (a) NCEP2 and (b) FGOALS-s2. The difference of the divergence between NCEP2 and FGOALS-s2 is shown in (c). The dotted regions are where the differences are statistically significant at the 10% level.

cluding dynamical and thermal feedback) are the key processes to improve the model's performance with respect to jet streams. These interactions may be different in different phases of atmospheric oscillations, e.g. the Arctic Oscillation (AO) and Pacific Decadal Oscillation (PDO), since STEA or the jet streams may change accordingly. Chang and Fu (2002, 2003) investigated the relationship between the storm track and AO/PDO. They concluded that the storm track may become stronger and shift poleward in the positive phase of AO, but in the positive phase of PDO it will move equatorward. The East Asian winter monsoon (EAWM) is also closely related to the AO over the decadal time scale (Jhun and Lee, 2004). As an important component of the EAWM, the EASJ is also connected to the AO. Hence, the interactions between STEA and the EASJ deserve further investigation.

Acknowledgements. This work was jointly supported by the National High Technology Research and Development Program of China (Grant No. 2010AA012304), the National Program on Key Basic Research Project of China (Grant No. 2010CB951904), the National Natural Science Foundation of China project (Grant No. 41125017), and the "Strategic Priority Research Program – Climate Change: Carbon Budget and Related Issues" of the Chinese Academy of Sciences (Grant No. XDA05110301). The authors acknowledge the IAP/LASG for supporting the CMIP5 experiments for IPCC AR5 and releasing model data to the climate research community.

REFERENCES

Bao, Q., and Coauthors, 2013: The flexible global ocean-atmosphere-land system model spectral version: FGOALS-s2. *Adv. Atmos. Sci.,* doi: 10.1007/s00376-012-2113-9.

Cai, Q., T. Zhou, B. Wu, B. Li, and L. Zhang, 2011: The East Asian subtropical westerly jet and its interannual variability simulated by a climate system model FGOALS_gl. *Acta Oceanologica Sinica*, **33**, 38–48.

(in Chinese)

Carillo, A., P. M. Ruti, and A. Navarra, 2000: Storm tracks and zonal mean flow variability: A comparison between observed and simulated data. *Climate Dyn.*, **16**, 219–228.

Chang, E. K. M., and Y. Fu, 2002: Interdecadal variations in Northern Hemisphere winter storm track intensity. *J. Climate*, **15**, 642–658.

Chang, E. K. M., and Y. Fu, 2003: Using mean flow change as a proxy to infer interdecadal storm track variability. *J. Climate*, **16**, 2178–2196.

Du, Y., Y. Zhang, and Z. Xie, 2008: Impacts of longitude location changes of East Asian jet core on the precipitation distribution during meiyu period in middle-lower reaches of Yangtze River valley. *Acta Meteorologica Sinica*, **66**, 566–576. (in Chinese)

Du, Y., Y. Zhang, and Z. Xie, 2009: Location variation of the East Asia subtropical westerly jet and its effect on the summer precipitation anomaly over eastern China. *Chinese J. Atmos. Sci.*, **33**, 581–592. (in Chinese)

Guo, L., Y. Zhang, B. Wang, L. Li, T. Zhou, and Q. Bao, 2008: Simulations of the East Asian subtropical westerly jet by LASG/IAP AGCMs. *Adv. Atmos. Sci.*, **25**, 447–457, doi: 10.1007/s00376-008-0447-0.

Hoskins, B. J., I. N. James, and G. H. White, 1983: The shape, propagation and mean-flow interaction of large-scale weather systems. *J. Atmos. Sci.*, **40**, 1595–1612.

Jhun, J. G., and E. J. Lee, 2004: A new East Asian winter monsoon index and associated characteristics of the winter monsoon. *J. Climate*, **17**, 711–726.

Kanamitsu, M., W. Ebisuzaki, J. Woollen, S.-K. Yang, J. J. Hnilo, M. Fiorino, and G. L. Potter, 2002: NCEP–DOE AMIP-II reanalysis (R-2). *Bull. Amer. Meteor. Soc.*, **83**, 1631–1643.

Koch, P., H. Wernli, and H. C. Daves, 2006: An event-based jet-stream climatology and typology. *Int. J. Climatol.*, **26**, 283–301.

Kuang, X., Y. Zhang, J. Liu, and L. Guo, 2009: A numerical study of the effect of anomalous surface heating in the Kuroshio current region in winter on the East Asian subtropical westerly jet. *Chinese J. Atmos. Sci.*, **33**, 81–89. (in Chinese)

Lee, S., and H. Kim, 2003: The dynamical relationship between subtropical and eddy-driven jets. *J. Atmos. Sci.*, **60**, 1490–1503.

Li, C., J. Wang, S. Lin, and H. Cho, 2004: The relationship between East Asian summer monsoon activity and northward jump of the upper westerly jet location. *Chinese J. Atmos. Sci.*, **28**, 641–658. (in Chinese)

Li, J., R. Yu, and T. Zhou, 2005: Why is there an early spring cooling shift downstream of the Tibetan Plateau? *J. Climate*, **18**, 4660–4668.

Liang, X., and W. Wang, 1998: Association between China monsoon rainfall and tropospheric jets. *Quart. J. Roy. Meteor. Soc.*, **124**, 2597–2623.

Liao, Q., S. Gao, H. Wang, and S. Tao, 2004: Anomalies of the extratropical westerly jet in the North Hemisphere and their impacts on East Asian summer monsoon climate anomalies. *Chinese Journal of Geophysics*, **47**, 10–18. (in Chinese)

Liu, X., and M. Tang, 1996: On the critical height of the effect of Qinghai-Xizang Plateau uplift on the atmosphere. *Plateau Meteorology*, **15**, 131–140. (in Chinese)

Manabe, S., and T. B. Terpstra, 1974: The effects of mountains on the general circulation of the atmosphere as identified by numerical experiments. *J. Atmos. Sci.*, **31**, 3–42.

Ren, X., and Y. Zhang, 2007: Western Pacific jet stream anomalies at 200 hPa in winter associated with oceanic surface heating and transient eddy activity. *Acta Meteorologica Sinica*, **21**, 277–289.

Ren, X., X. Yang, and C. Chu, 2010a: Seasonal variations of the synoptic-scale transient eddy activity and polar front jet over East Asia. *J. Climate*, **23**, 3222–3233.

Ren, X., X. Yang, T. Zhou, and J. Fang, 2010b: Diagnostic comparison of the East Asian subtropical jet and polar-front jet: Large-scale characteristics and transient eddy activities. *Acta Meteorologica Sinica*, **68**, 1–11.

Schiemann, R., D. Luthi, and C. Schar, 2009: Seasonality and interannual variability of the westerly jet in the Tibetan Plateau region. *J. Climate*, **22**, 2940–2957.

Sheng, C., 1986: *An Introduction to the Climate of China.* Science Press, Beijing, 85–89. (in Chinese)

Strong, C., and R. E. Davis, 2007: Winter jet stream trends over the Northern Hemisphere. *Quart. J. Roy. Meteor. Soc.*, **133**, 2109–2115.

Strong, C., and R. E. Davis, 2008: Variability in the position and strength of winter jet stream cores related to Northern Hemisphere teleconnections. *J. Climate*, **21**, 584–592.

Tao, S., Y. Zhao, and X. Chen, 1958: The relationship between Meiyu in far east and the behavior of circulation over Asia. *Acta Meteorologica Sinica*, **29**, 119–134. (in Chinese)

Watanabe, M., 2004: Asian jet waveguide and a downstream extension of the North Atlantic oscillation. *J. Climate*, **17**, 4674–4691.

Wu, W., J. He, H. S. Chung, C. H. Cho, and R. Lu, 2006: The relationship between the East Asian upper-tropospheric jet stream in summer and climatic characteristics of synoptic-scale disturbances. *Climatic and Environmental Research*, **11**, 525–534. (in Chinese)

Xiang, Y., and X. Yang, 2012: The effect of transient eddy on interannual meridional displacement of summer East Asian subtropical jet. *Adv. Atmos. Sci.*, **29**, 484–492, doi: 10.1007/s00376-011-1113-5.

Xin, X., R. Yu, T. Zhou, and B. Wang, 2006: Drought in late spring of South China in recent decades. *J. Climate*, **19**, 3197–3206.

Yang, J., Q. Bao, X. Wang, and T. Zhou, 2012: The tropical intraseasonal oscillation in SAMIL coupled

and uncoupled general circulation models. *Adv. Atm. Sci.*, **29**(3), 529–543, doi: 10.1007/s00376-011-1087-3.

Yeh, D., S. Tao, and M. Li, 1958: The abrupt change of circulation over Northern Hemisphere during June and October. *Acta Meteorologica Sinica*, **29**, 249–263. (in Chinese)

Yu, R., and T. Zhou, 2004: Impacts of winter-NAO on March cooling trends over subtropical Eurasia continent in the recent half century. *Geophys. Res. Lett.*, **31**, L12204, doi: 10.1029/2004GL019814.

Yu, R., and T. Zhou, 2007: Seasonality and three dimensional structure of the interdecadal change in East Asian monsoon. *J. Climate*, **20**, 5344–5355.

Zhang, L., and Coauthors, 2010: The annual modes of tropical precipitation simulated by the LASG/IAP coupled ocean-atmosphere model FGOALS_s1.1. *Acta Meteorologica Sinica*, **24**(2), 189–202.

Zhang, Y., and X. Kuang, 2006: Simulation of seasonal variation of the East Asian subtropical westerly jet in a coupled climate system model FGCM0. *Chinese J. Atmos. Sci.*, **30**, 1177–1188. (in Chinese)

Zhang, Y., X. Kuang, W. Guo, and T. Zhou, 2006: Seasonal evolution of the upper-tropospheric westerly jet core over East Asia. *Geophys. Res. Lett.*, **33**, L11708, doi: 10.1029/2006GL026377.

Zhang, Y., D. Wang, and X. Ren, 2008a: Seasonal variation of the meridional wind in temperate jet stream and its relationship to the Asian monsoon. *Acta Meterologica Sinica*, **66**, 707–715. (in Chinese)

Zhang, Y., M. Takahashi, and L. Guo, 2008b: Analysis of the East Asian subtropical westerly jet simulated by CCSR/NIES/FRCGC coupled climate system model. *J. Meteor. Soc. Japan*, **86**, 257–278.

Zhou, T., and R. Yu, 2005: Atmospheric water vapor transport associated with typical anomalous summer rainfall patterns in China. *J. Geophys. Res.*, **110**, D08104, doi: 10.1029/2004JD005413.

Zhou, T., and Coauthors, 2005: The climate system model FGOALS s using LASG/IAP spectral AGCM SAMIL at its atmospheric component. *Acta Meteorologica Sinica*, **63**(5), 702–715.

Zhou, T., F. Song, and X. Chen, 2013: The historical evolutions of global and regional surface air temperature simulated by FGOALS-s2 and FGOALS-g2: How reliable are model results? *Adv. Atmos. Sci.*, doi: 10.1007/s00376-013-2205-1.

Zou, J., J. Jiang, and M. Wang, 1990: *Aeroclimatology*. China Meteorological Press, Beijing, 202–212. (in Chinese)